Non-linear Theory and Experiment of Collective Free Electron Lasers

J.S. Wurtele, R. Chu and J. Fajans

October 1989

Department of Physics

and

Plasma Fusion Center

Massachusetts Institute of Technology
Cambridge, Massachusetts 02139 USA

Non-linear Theory and Experiment of Collective Free Electron Lasers

Jonathan S. Wurtele and Ronson Chu

Dept. of Physics and Plasma Fusion Center

Massachusetts Institute of Technology

Cambridge MA 02139

and

Joel Fajans

Dept. of Physics

University of California, Berkeley

Berkeley CA 94720

1

Abstract

A theoretical and experimental study of the nonlinear performance of a free electron laser (FEL) amplifier operating in the collective (Raman) regime is reported. The FEL generates up to ~ 100KW of RF power at a frequency of 9.3GHz and an efficiency of $\sim 10\%$. Power saturation, efficiency, and synchrotron oscillations are studied as a function of RF input power, electron beam energy, current, wiggler field amplitude, and axial distance within the helical wiggler. The influences of the nonlinear electron motion in the ponderomotive potential and space charge waves are studied by measurements of the dependence of gain and efficiency on the initial radiation intensity. Excellent agreement with a nonlinear theory that takes cognizanse of electron trapping in the combined ponderomotive and space charge potential well is obtained.

I. Introduction

Free electron lasers (FELs) are currently under investigation because of their remarkable properties, which include their high efficiencies and output powers, their potential as coherent short wavelength sources, and their inherent frequency tunability. Subsequent to the original envisioning[1,2] of the FEL and the first proof-of-principle experiments,[3] detailed comparisons of experiment and theory have been made in the linear[4,5] and nonlinear regimes.[6,7]

In this paper we study the non-linear behavior of a microwave FEL. Previously, the small signal linear gain behavior of this device was investigated,[5] and is now well understood. Further investigations found good agreement between numerical simulation and measurements of the nonlinear amplitude and phase of the RF wave.[6] Here we examine the influence of RF input power on the saturation and detuning characteristics of the laser, and examine the power as a function of the beam current and the wiggler field amplitude and length. The physics of our collective FEL is well described by electron trapping in the potential formed by the combined action of the ponderomotive and self-consistent space charge forces.

The major differences between the microwave regime FEL theory studied here and the standard optical (Compton) regime FEL theory[8-10] are corrections for the excitation of a collective space charge wave on a finite radius beam propagating in a waveguide, the transverse structure of the waveguide mode,[11,12] three-dimensional wiggler fields, the presence of an axial guide magnetic field, and the relatively low velocity ($v/c \sim 0.6$) of the electron beam. Three-dimensional effects are included by using appropriately calculated coupling

coefficients as input parameters and solving transcendental expressions for the transverse electron motion.[13] These extended one dimensional model input parameters are found analytically through the evaluation of the overlap between the waveguide mode and electron beam, and the evaluation of space charge reduction factors. The FEL equations are solved using a numerical simulation that tracks macro-particles in a single ponderomotive wavelength. The simulation is itself one-dimensional, and propagates only the TE_{11} waveguide mode. There are no adjustable parameters. Parts of this paper expand on previous comparisons between experiment and theory reported earlier,[6,8] and parts report new studies of the influence of input wave power on the FEL efficiency and gain.

Section 2 derives our nonlinear model and numerical simulation. Section 3 discusses the space charge wave, which is particularly important in our parameter regime. Section 4 contains the linearization of the model and comparison with previous linear theories. Section 5 compares the experimental and theoretical results, and reports the first measurements of the shift in optimum detuning and changes in efficiency scaling which result from increasing the RF input power.

II. Derivation of the Nonlinear Model

In this section we derive the nonlinear model of the FEL for the parameter regime of our microwave FEL experiment. The model couples single particle orbits in combined helical and axial magnetic fields with the the slowly varying amplitude and phase of the TE_{11} mode in a circular waveguide. The nonlinear equations of motion are one dimensional, but allow for the effects of transverse field variations through the evaluation of waveguide mode-beam overlap integrals and space charge reduction factors. The influence of the three dimensional wiggler fields on the electron orbits is analyzed by solving the well-known transcendental equations relating the energy γ and the normalized perpendicular and parallel velocities $\beta_\perp$ and $\beta_\parallel$ for an electron on an ideal orbit. We do not assume that $\gamma \gg 1$.

A. Particle Equations

Electrons orbit in the combined axial magnetic field

$$\vec{B}_0 = B_0 \hat{z} \tag{1}$$

and helically polarized wiggler field given by

$$\vec{B}_w(r, \phi, z) = 2B_w \left(-I_1'(\lambda) \sin(k_w z - \phi)\hat{r} + \frac{I_1(\lambda)}{\lambda} \cos(k_w z - \phi)\hat{\phi} - I_1(\lambda) \cos(k_w z - \phi)\hat{z} \right) \tag{2}$$

where $\lambda = k_w r$, $k_w = 2\pi/l$ is the wiggler wavenumber, I_1 is the modified Bessel function, ' denotes derivative with respect to the total argument, and we use cylindrical coordinates

(r, ϕ, z). Neglecting the influence of the radiation field, and assuming an ideal wiggler entrance, the electron orbits are described by[5]

$$\vec{\beta}_\perp = \beta_\perp \left(\sin(k_w z - \phi)\hat{r} - \cos(k_w z - \phi)\hat{\phi} \right) , \qquad (3)$$

where the normalized perpendicular velocity $\beta_\perp$ is found from the simultaneous solution of the equations

$$\frac{\dot{\beta}_\perp}{\beta_\parallel} = \frac{2\Omega_w c k_w I_1(\lambda)/\lambda}{c\beta_\parallel k_w \gamma - \Omega_0 - 2\Omega_w c k_w I_1(\lambda)} \qquad (4)$$

and

$$\beta_\parallel = \sqrt{1 - \frac{1}{\gamma^2} - \beta_\perp^2} . \qquad (5)$$

In Eq. 4, the velocities $\beta_\perp$ and $\beta_\parallel$ are normalized by the speed of light c, Ω_w, Ω_0 are the wiggler and axial cyclotron frequencies, $\gamma = 1 + eV/m_0 c^2$ is the beam energy, and $\lambda = \beta_\perp/\beta_\parallel = \pm k_w r$ is the normalized size of the orbit, with $\lambda = -k_w r$ if $\Omega_0 > \gamma k_w \beta_\parallel c$ and $\lambda = +k_w r$, if $\Omega_0 < \gamma k_w \beta_\parallel c$. We assume that electrons remain on these orbits during the FEL interaction. Thus we neglect the detailed effects of the precession due to off axis injection[14] and emittance; this is a good approximation for the high quality electron beam used in this experiment. In addition, the direct influence of the radiation field on the perpendicular motion is very small for the low powers at which this FEL operates. Thus the radiation field influences the particle motion only through the energy relation $d\gamma/dt \sim \vec{v} \cdot \vec{E}$; consequently, the perpendicular and parallel energies evolve so that the electron stays on the orbit given by the Eqs. 4- 5.

With the time t replaced by the axial position z as the independent variable, the electron

(charge $-e$, mass m_0) energy evolves according to

$$\frac{d\gamma}{dz} = -\frac{e}{m_0 c^2}\frac{\beta_\perp}{\beta_\parallel}\frac{A(z)Z_0 k_0}{k_\perp}\left(\frac{J_1(\alpha)}{\alpha}\sin(k_w z - \phi(z))\cos(\theta_s + \phi(z))\right.$$

$$\left. + J_1'(\alpha)\cos(k_w z - \phi(z))\sin(\theta_s + \phi(z))\right) - \frac{e}{m_0 c^2}E_z, \qquad (6)$$

where $\theta_s = k_z z + \varphi(z) - \omega t(z)$, the amplified wave frequency, axial wavenumber and perpendicular wave number are given by ω, k_z, and $k_\perp$, respectively, $k_0 = \omega/c$ is the normalized frequency, E_z is the axial component of the electric field due to the beam bunching, $\alpha = k_\perp r$, the impediance of free space is Z_0, and J_1 is a Bessel function. In deriving Eq. 6, the transverse components of the waveguide mode are taken from Table 1. Furthermore, the amplified wave amplitude, $A(z)$, and phase, $\varphi(z)$, are assumed to be slowly varying on the spatial scale $\lambda_s = 2\pi c/\omega$. The radial space charge field also contributes to the electron motion, but does not generate a large slowly varying term in the energy equation. As described below, the expression for E_z includes the influence of the conducting waveguide wall through an appropriately calculated coupling parameter.

For our experiment, the electron beam is small compared to the radial gradients in the transverse radiation field, so that $\alpha \ll 1$ (typically, $\alpha \approx .36$). With the simplification that $J_1(\alpha) \approx \alpha/2$, the energy equation reduces to

$$\frac{d\gamma}{dz} = -\frac{e}{m_0 c^2}\frac{\beta_\perp}{\beta_\parallel}\frac{A(z)Z_0 k_0}{2k_\perp}\sin\psi - \frac{e}{m_0 c^2}E_z, \qquad (7)$$

where ψ is the slowly varying phase of the particle in the ponderomotive wave. It is convenient to introduce the dimensionless field amplitude

$$a_s = \frac{\sqrt{PZ_0}}{m_0 c^2/e} \qquad (8)$$

and the length scale

$$C = \sqrt{\frac{k_0 p_{11}'^2}{2\pi k_z r_g^2 (p_{11}'^2 - 1) J_1^2(p_{11}')}} , \qquad (9)$$

where r_g is the waveguide radius, p_{11}' is the first zero of $J_1'(z)$, and P is the EM wave power. With these definitions, the electron energy and phase evolve according to

$$\frac{d\gamma}{dz} = -C \frac{\beta_\perp}{\beta_\parallel} a_s \sin\psi - \frac{e}{m_0 c^2} E_z , \qquad (10)$$

and

$$\frac{d\psi}{dz} = k_w + k_z - \frac{\omega}{c\beta_\parallel} + \frac{d\varphi}{dz} . \qquad (11)$$

B. Field Equations

The Maxwell equation

$$-\nabla^2 \vec{E} + \nabla(\nabla \cdot \vec{E}) - \frac{\omega^2}{c^2}\vec{E} = -\mu_0 \frac{\partial \vec{J}}{\partial t} \qquad (12)$$

for the electric field can be simplified by assuming that the electric field is composed of a vacuum waveguide mode with a slowly varying amplitude and phase, as shown in Table 1, and a space charge field $\vec{E}_{sc}(\phi, r, z)$, also with a slow z dependence. The divergence free electric field of the TE_{11} mode satisfies

$$\begin{aligned}
-\nabla^2 \vec{E} - \frac{\omega^2}{c^2}\vec{E} &= 2k_z \frac{Z_0 k_0}{k_\perp}\left(-\frac{J_1(k_\perp r)}{k_\perp r}\sin(\theta_s - \phi)\hat{r} + J_1'(k_\perp r)\cos(\theta_s - \phi)\hat{\phi}\right)\frac{dA}{dz} \\
&\quad -2k_z A \frac{Z_0 k_0}{k_\perp}\left(\frac{J_1(k_\perp r)}{k_\perp r}\cos(\theta_s - \phi)\hat{r} + J_1'(k_\perp r)\sin(\theta_s - \phi)\hat{\phi}\right)\frac{d\varphi}{dz} \\
&= -\mu_0 \frac{\partial \vec{J}}{\partial t} .
\end{aligned} \qquad (13)$$

TE$_{11}$ Waveguide Mode Field Components	
E_r	$A(z)(k_0 Z_0/k_\perp^2 r)J_1(k_\perp r)\cos(\theta_s + \phi)$
E_ϕ	$-A(z)(k_0 Z_0/k_\perp)J_1'(k_\perp r)\sin(\theta_s + \phi)$
E_z	0
H_r	$A(z)(k_z/k_\perp)J_1'(k_\perp r)\sin(\theta_s + \phi)$
H_ϕ	$A(z)(k_z/k_\perp^2 r)J_1(k_\perp r)\cos(\theta_s + \phi)$
H_z	$-A(z)J_1(k_\perp r)\cos(\theta_s + \phi)$
$Z_{11} = k_0 Z_0/k_z$	
$p_{11}' = 1.841 = k_\perp r_g$	
$Power$	$A^2(z)Z_{11}k_z^2\pi({p_{11}'}^2 - 1)J_1^2(p_{11}')/2k_\perp^4$

Table 1: TE$_{11}$ waveguide mode.

Note that the vacuum relation $\omega^2/c^2 = k_0^2 = k_z^2 + k_\perp^2$ has been used.

The current can be expressed as a function of z,

$$\vec{J} = -e \sum_i \vec{\beta}_i(z)\delta(\vec{r}_\perp - \vec{r}_{wi}(z))\delta(t - t_i(z))/\beta_{\|i}(z), \tag{14}$$

where $\vec{r}_{wi}(z)$ is the transverse position of a particle, the index i is a particle label, and $\beta_\perp$ and $\beta_\|$ are found from Eq. 4 and Eq. 5. Multiplication of Eq. 13 by

$$\left(-\frac{J_1(k_\perp r)}{k_\perp r} \sin(\theta_s - \phi)\hat{\mathbf{r}} + J_1'(k_\perp r) \cos(\theta_s - \phi)\hat{\phi} \right),$$

using Eq. 14, and integrating over the waveguide cross section yields

$$\frac{k_0 k_z Z_0}{k_\perp^3} \pi({p_{11}'}^2 - 1)J_1^2(p_{11}')\frac{dA}{dz} = \frac{\omega\mu_0 I}{2} \left\langle \frac{\beta_{\perp i}}{\beta_{\|i}} \sin\psi_i \right\rangle \tag{15}$$

where I is the current. The average of a function F of the particle variables $(\beta_\perp, \beta_\|, \gamma, \psi)$ is defined as

$$\left\langle F(\beta_\perp, \beta_\|, \gamma, \psi) \right\rangle = \frac{1}{N_p} \sum_{i=1}^{N_p} F(\beta_{\perp i}, \beta_{\|i}, \gamma_i, \psi_i), \tag{16}$$

where N_p is the number of particles in one ponderomotive wavelength.

In terms of the normalized variables,

$$\frac{da_s}{dz} = \frac{2\pi C I}{I_A} \left\langle \frac{\beta_\perp}{\beta_\|} \sin\psi \right\rangle, \tag{17}$$

where C is defined in Eq. 9, and $I_A = 17\text{kA}$ is the Alfen current. The phase evolution is found through multiplication of Eq. 13 by the factor

$$\left(\frac{J_1(k_\perp r)}{k_\perp r} \cos(\theta_s - \phi)\hat{\mathbf{r}} + J_1'(k_\perp r) \sin(\theta_s - \phi)\hat{\phi} \right),$$

and integration over the waveguide cross section, to be

$$\frac{d\varphi}{dz} = \frac{2\pi CI}{I_A a_s} \left\langle \frac{\beta_\perp}{\beta_\parallel} \cos\psi \right\rangle .$$ (18)

The space charge wave field, which results from the beam bunching at the ponderomotive wavelength, is assumed to be of the form

$$\vec{E}_{sc} = \sum_n \vec{E}_{nc}(\mathbf{x}_\perp, z) \cos n\psi + \vec{E}_{ns}(\mathbf{x}_\perp, z) \sin n\psi ,$$ (19)

where the axial variation of E_{ns} and E_{nc} is slow compared to the radiation wavelength. The z component of the space charge wave then evolves, from Eq. 12 as

$$\left(\nabla^2 + \frac{\omega^2}{c^2} \right) E_z = \frac{1}{\epsilon_0} \left(\frac{\partial\rho}{\partial z} + \mu_0\epsilon_0 \frac{\partial J_z}{\partial t} \right) .$$ (20)

By expanding the current and density in a series as in Eq. 19, using the continuity equation and equating the Fourier components on both sides of Eq. 20, it can be shown that

$$\left(1 - \frac{\gamma_p^2}{n^2(k_z + k_w)^2} \nabla_\perp^2 \right) E_{znc} = -\frac{\rho_{ns}}{\epsilon_0 n(k_z + k_w)} ,$$ (21)

$$\left(1 - \frac{\gamma_p^2}{n^2(k_z + k_w)^2} \nabla_\perp^2 \right) E_{zns} = \frac{\rho_{nc}}{\epsilon_0 n(k_z + k_w)} ,$$ (22)

where n is the harmonic number, ρ_{nc} and ρ_{ns} are the Fourier components of the charge density ρ, $\gamma_p = 1/\sqrt{1 - v_p^2/c^2}$, and $v_p = \omega/(k_z + k_w)$ is the phase velocity of the ponderomotive wave.

For simplicity, the normalized electric field which enters the simulation is not found by solving the above equations for E_z. Instead, as in earlier work,[4,6] a space charge reduction factor, p_1, is utilized. This factor, which is ~ 0.5 for the parameters of our experiment, can be found in the literature[16] (with corrections for $\gamma > 1$) for the case of an unbunched

electron beam with a uniform density profile. Recently, several careful treatments of the space-charge wave in the FEL have been made.[17-19] All of these treatments indicate that the model presented here is quite satisfactory for the parameter regime of this experiment. The electric field used in the one dimensional simulation presented here is then

$$\frac{E_z}{m_0 c^2/e} = \frac{2p_1^2 \omega_{p0}^2}{c^2(k_z + k_w)} \sum_{n=1}^{N_h} \frac{\langle \sin n\psi \rangle \cos n\psi - \langle \cos n\psi \rangle \sin n\psi}{n} \tag{23}$$

where n is the harmonic number, r_e is the radius of the beam, $\omega_{p0}^2 = e^2 n_0/\epsilon_0 m_0$, and $n_0 = I/ec\pi r_e^2 \beta_{\|0}$. For the parameters of interest here, the factor p_1 varies only slightly for differing harmonics n. In general, p_1 cannot be removed from the summation and will be a function of n. For experiments with strong space charge forces, such as the one herein, the use of only the first harmonic will lead to erroneous results in the nonlinear regime.

In summary, Eqs. 4, 5, 10, 11, 17, 18, and 23 constitute the model of the FEL which is implemented numerically in this study of nonlinear FEL phenomena. The simulation assumes that as the electrons exchange energy with the wave, they do not deviate from the ideal wiggler orbits given by the solution to Eqs. 4 and 5. We ignore the influence of the transverse gradients of both the radiation field and the space charge wave on the amplitude of the perpendicular motion. Note that since $\lambda = k_w r_e < 1$, $I_1(\lambda) \approx \lambda/2$, the right hand side of Eq. 4 is only a weak function of λ unless the electron is close to resonance. As the power approaches saturation, the fundamental ($n = 1$) and the harmonics ($n > 1$) of the space charge wave generate rather complicated particle orbits.

III. Space Charge Forces in the Collective FEL

Examination of the coupled FEL equations shows that the particle bunching in the ponderomotive beat wave between the wiggler and radiation fields will result in space charge forces which, for the low energy beam of this experiment, can be comparable in strength to the ponderomotive force. This is apparent in the Fig. 1, where the particle phase space (γ, ψ) and force $(d\gamma/dz, \psi)$ are plotted at four axial positions in the 2m wiggler. Initially, in Fig. 1a–b, the particles are unbunched and the force is nearly zero; then, for small bunching, Fig. 1c–d, the force is nearly sinusoidal. The power saturates near $z = 1$m, and subsequently the force has large harmonic content (Fig. 1e–f). The phase space portraits are seen to be substantially distorted from the usual FEL pendulum motion, where after sturation, tight bunches would form inside clearly defined seperatix. The power and phase evolution for these runs are shown in Fig. 2a–b.

The strong influence of the space charge forces on the particle motion is illustrated in Fig. 3a–b. Here the electrons are injected at the resonant energy, where the Raman regime FEL gain is small. The input power is sufficient to produce at least one synchrotron oscillation during the interaction. At high current, the space charge is strong enough to debunch the beam and the particles oscillate only slightly (Fig. 3a), while at low current, the particles move on pendulum-like orbits (Fig. 3b). Approximating the space charge wave with only one harmonic yields results different from the simulation, (which includes four harmonics,) by a few percent before saturation, and by 10–15 percent after saturation. Efficiency en-

hancement schemes are also rendered more difficult by the space charge debunching. For the low wiggler fields of this experiment, the product $\gamma\beta_\perp \ll 1$, and efficiency enhancement must rely on a wiggler wavelength downtaper. Numerous numerical schemes were examined and, for our typical system parameters, detrapping during the taper severely limited the efficiency. Thus our studies indicate that FEL operating deep in the Raman regime will be difficult to taper.

IV. Linearized Equations

The FEL interaction can be described by particle bunching in the ponderomotive wave coupled to concomitant field growth driven by the synchronous component of the current density. The bunching arises primarily from the phase change due to an energy shift. Linearization of the single particle model with space charge has been performed for planar and helical wigglers[20] and for circular wiggler,[21] but not for the helical wiggler and guide field case discussed here. We will follow the formalism of these references, which may be consulted for further details . We will find that the linearization of our model, under the (good) approximation that the dominant term in the field equation is the phase bunching which arise from energy changes, results in a cubic dispersion relation found previously[22] using kinetic theory.

For simplicity, the FEL equations may be written in the complex form as

$$\frac{d\gamma}{dz} = \frac{iC\beta_\perp}{2\beta_\parallel}ae^{i\theta} - \frac{i\omega_{p0}^2 p_1^2}{c^2(k_z + k_w)} \sum_n \frac{e^{in\theta}\left\langle e^{-in\theta}\right\rangle}{n} + c.c. , \tag{24}$$

$$\frac{d\theta}{dz} = k_w + k_z - \frac{\omega}{c\beta_\parallel}, \tag{25}$$

$$\frac{da}{dz} = \frac{i2\pi CI}{I_A} \left\langle \frac{\beta_\perp}{\beta_\parallel} e^{-i\theta} \right\rangle, \tag{26}$$

where the complex field $a = a_s e^{i\phi}$. The linearization proceeds by defining

$$\Delta K = k_w + k_z - \frac{\omega}{c\beta_{\parallel 0}}, \tag{27}$$

$$\theta = \theta_0 + \Delta K z + \delta\theta, \tag{28}$$

$$\gamma = \gamma_0 + \delta\gamma, \tag{29}$$

$$\beta_\parallel = \beta_{\parallel 0} + \frac{\partial\beta_{\parallel 0}}{\partial\gamma}\delta\gamma, \tag{30}$$

$$\eta = \frac{2\pi CI}{I_A}. \tag{31}$$

The injected beam is initially unbunched:

$$\left\langle e^{i(\theta_0 + \Delta K z)} \right\rangle = 0. \tag{32}$$

The dispersion relation is easily found by assuming exponential forms for the perturbations,

$$\delta\gamma = \overline{\delta\gamma} e^{i(\theta_0 + \Delta K z + \Gamma z)} + c.c., \tag{33}$$

$$\delta\theta = \overline{\delta\theta} e^{i(\theta_0 + \Delta K z + \Gamma z)} + c.c., \tag{34}$$

$$a = \overline{a} e^{i\Gamma z}. \tag{35}$$

Combining the equations for $\delta\gamma$ and $\delta\theta$ and averaging over the particle distribution yields an expression for the phase bunching

$$\left\langle -i\overline{\delta\theta} \right\rangle = -\frac{\overline{a}}{\chi_\parallel} \left\langle \frac{\omega C\beta_{\perp 0}}{2c\beta_{\parallel 0}^3} \frac{\partial\beta_{\parallel 0}}{\partial\gamma} / (\Delta K + \Gamma)^2 \right\rangle, \tag{36}$$

where

$$\chi_\| = 1 - \frac{\omega_{po}^2 p_1^2}{(k_z + k_w)c^2} \left\langle \frac{\omega}{c\beta_{\|0}^2} \frac{\partial \beta_{\|0}}{\partial \gamma} / (\Delta K + \Gamma)^2 \right\rangle . \tag{37}$$

Note that, in the absence of the radiation field, Eq. 36 yields $\chi_\| = 0$, which becomes, with $\omega/(k_z + k_w) \approx c\beta_{\|0}$

$$\frac{p_1^2 \omega_{po}^2}{\beta_{\|0}(\Delta K + \Gamma)^2 c^2} \frac{\partial \beta_{\|0}}{\partial \gamma} = 1 . \tag{38}$$

Solving Eq. 38 for Γ yields the longitudinal beam plasma frequency (along with the arbitrary shift ΔK).

Employing Eq. 36 in the linearized equations for $\overline{\delta\gamma}$, $\overline{\delta\theta}$, and $\bar{a}$ results in the dispersion relation

$$-\frac{2\pi CI}{I_A \Gamma} \left(\left\langle \frac{\beta_{\perp0}}{\beta_{\|0}} \frac{\omega C \beta_{\perp0}}{2c\beta_{\|0}^3} \frac{\partial \beta_{\|0}}{\partial \gamma} / (\Delta K + \Gamma)^2 \right\rangle \right.$$
$$\left. + \frac{\omega_{po}^2 p_1^2}{(k_z + k_w)c^2 \chi_\|} \left\langle \frac{\omega C \beta_{\perp0}}{2c\beta_{\|0}^3} \frac{\partial \beta_{\|0}}{\partial \gamma} / (\Delta K + \Gamma)^2 \right\rangle \left\langle \frac{\beta_{\perp0}}{\beta_{\|0}} \frac{\omega}{c\beta_{\|0}^2} \frac{\partial \beta_{\|0}}{\partial \gamma} / (\Delta K + \Gamma)^2 \right\rangle \right) = 1. (39)$$

In deriving Eq. 39, We only included the $\delta\theta$ term in the linearized a equation. There is also a $\delta\gamma$ term in the a equation which, if included, would slightly modify Eq. 39. For a cold, tenuous beam, the factor ΔK is equal for each electron, and only lowest order in ω_{po}^2 need be retained after multiplication of Eq. 39 by $\chi_\|$. Then a simplified cubic dispersion relation can be derived:

$$\Gamma^3 + 2\Delta K \Gamma^2 + (\Delta K^2 - \frac{\omega}{c\beta_{\|0}^2} \frac{\partial \beta_{\|0}}{\partial \gamma} \frac{\omega_{po}^2 p_1^2}{(k_z + k_w)c^2}) \Gamma + \frac{\pi C^2 \beta_{\perp0}^2 I \omega}{\beta_{\|0}^4 c I_A} \frac{\partial \beta_{\|0}}{\partial \gamma} = 0 . \tag{40}$$

The factor $\frac{\partial \beta_{\|0}}{\partial \gamma}$ can be expressed, using Eqs. 4 and 5 and restricting to the limit $\lambda \ll 1$,

as

$$\frac{\partial \beta_{\|0}}{\partial \gamma} = \frac{1}{\gamma \beta_{\|0}} \left(\frac{1}{\gamma_{\|}^2} + \frac{x}{1-x} \right) \tag{41}$$

where $\gamma_{\|}^2 = 1/(1 - \beta_{\|0}^2)$ and

$$x = \frac{c^2 k_w^2 a_w^2 \Omega_0}{(c\beta_{\|} k_w \gamma - \Omega_0)^3} . \tag{42}$$

With this expression for $\frac{\partial \beta_{\|0}}{\partial \gamma}$ the cubic dispersion relation Eq. 40 is identical to the cubic dispersion relation previously obtained by previous authors[22] and the space charge wave may be unstable in a suitable parameter regime.[23]

V. Comparisons with Experiment

The FEL experiment has been described in detail elsewhere,[5,6] and the reader is refered to these references for a detailed description of the apparatus. Free electron laser physics is studied here by measuring the output RF power with varying beam energy, beam current, wiggler field, input RF power level and interaction length. The wiggler has a 3.3cm period with an adiabatic entrance over six periods. The length of the interaction region is adjusted by an axially moveable "kicker" magnet that deflects the beam into the waveguide wall.

The input power source is a 9.3GHz high power (~ 30KW) short pulse magnetron, which saturates the FEL at approximately 1m. The axial location of saturation can be shifted by changing the wiggler field, as shown in Fig. 4, where the power is plotted as a function of axial position for three wiggler field amplitudes. The general behaviour of the experiment is reproduced by the theory, but at the stronger wiggler fields the experimental measurements are larger by $\sim 15\%$ than are predicted.

The output powers shown in Fig. 4 are for the fixed beam voltage V that gives the greatest gain at the beginning of the wiggler ($z \lesssim 60$cm). We find that the voltage that yields the maximum output power increases steadily for interaction lengths longer than the saturation length. At the peak gain voltage, the FEL saturates at approximately $z \approx 115$cm, after which a synchrotron oscillation causes the output power to decrease. As shown by the simulations of Fig. 5, at higher beam voltages the FEL interaction proceeds more slowly, and saturation is delayed past $z = 115$cm. Thus, at large z the output power is maximized

at higher beam voltages.

This phenomenon is shown experimentally in Figs. 6 and 7. In Fig. 6, we plot the output power as a function of beam voltage for three axial positions. In both the data and in the simulation the voltage corresponding to peak gain increases $\sim 2\%$ as z increases from 81cm to 155cm. Figure 7 shows the voltage for peak gain as a function of interaction length between $z = 81$cm and $z = 155$cm.

The peak gain voltage depends on axial position past saturation. In addition, at high power, nonlinear phenomena exist well before saturation ($z \stackrel{<}{\sim} 60$cm). These effects cause the voltage that gives the maximum output power to differ from both the predictions of linear theory and from measurements at small input signals. For example, at 30KW the computed beam energy that maximizes the unsaturated gain is approximately 2% higher than is found with small signal linear theory. This effect is explained schematically in Fig. 8. The electron beam energy corresponding to peak linear gain, γ_g, is, in the Raman regime, upshifted from the resonant energy, γ_r, by a factor proportional to the beam plasma frequency. When the input power is small, the ponderomotive potential bucket height is also small compared to $\gamma_g - \gamma_r$. In this case the input beam energy corresponding to maximum unsaturated output power is just the γ_g from linear theory. However, when the input power is increased sufficiently, the trapping bucket approaches the linear optimized beam energy γ_g. When this occurs the output power can be increased by increasing the beam energy above the energy γ_g predicted by linear theory.

This effect is observed experimentally and is reproduced in the simulations. The dashed

line in Fig. 9 is the computed energy for peak gain as a function of the input power. For low power, the peak gain energy is equal to the linear regime peak gain energy. However, when the power is sufficiently large, (the bucket height is of order $\gamma_g - \gamma_r$), the input energy corresponding to peak gain increases.

Efficiency measurements constitute another test of nonlinear FEL theory. We find that the well known[13] theoretical collective regime efficiency scaling with current, $\eta \propto I^{1/2}$ is not observed for high input power and low beam current. Linear theory predicts that the difference $\gamma_g - \gamma_r$ also scales as $I^{1/2}$. As indicated in Fig. 8 , when the beam current is reduced, the γ_g of linear theory moves inside the ponderomotive bucket at $z = 0$, and then the peak gain energy is no longer γ_g. Under these conditions experiments and simulations show that more power can be extracted by increasing the initial beam energy. The efficiency is then only a weak function of the current. In Fig. 10 we plot the numerically predicted efficiency, on log-log scales, for two input powers, as a function of the beam current. The low input power line, marked with the dots, is linear. The high input power plot, marked by triangles, is linear at high current, but flattens at low current. The experimentally observed efficiency,[6] marked by the crosses, is taken at high power only. As expected, the efficiency is roughly flat over the measured beam current range.

VI. Conclusions

We find that our measurements of the spatial RF growth, saturation, and subsequent decay in our collective (Raman) free electron laser amplifier are well explained by a nonlinear

theory which takes into account electron trapping in the potential wells formed by the combined action of the ponderomotive and beam space charge forces. Scaling of the power and efficiency with electron beam current and voltage are likewise in agreement with theoretical predictions. Many of the results presented in this paper are for input powers comparable to the output power; however despite appearances, this is not an artificial regime. It is in fact precisely the operating regime of a low gain, multi-pass oscillator. The various energy shifts and scaling law changes demonstrated in this paper must be carefully considered when optimizing the behavior of such an oscillator.

VII.   Acknowledgments

References

[1] H. Motz, J. Appl. Phys. **22**, 527 (1951).

[2] R. M. Phillips, IRE Trans. Electron Devices **ED-7**, 231 (1960).

[3] L. R. Elias, W. Fairbank, J. Madey, H. A. Schwettman, and T. Smith, Phys. Rev. Lett. **36**, 717 (1976).

[4] T. J. Orzechowski, E. T. Scharlemann, B. Anderson, V. K. Neil, W. M. Fawley, D. Prosnitz, S. Yarema, D.B. Hopkins, A. C. Paul, A. M. Sessler, and J. S. Wurtele, IEEE Jour. Quan. Electron. **QE-21**, 831 (1985).

[5] J. Fajans, G. Bekefi, Y. Z. Yin, and B. Lax, Phys. Rev. Lett. **53**, 246 (1984) and J. Fajans and G. Bekefi, Phys. Fluids **26**, 1995 (1985).

[6] J. Fajans, J. S. Wurtele, G. Bekefi, D. K. Knowles, and K. Xu, Phys. Rev. Lett. **57**, 579 (1986).

[7] T. J. Orzechowski, B. R. Anderson, J. C. Clark, W. M. Fawley, A. C. Paul, D. Prosnitz, E. T. Scharlemann, S. M. Yarema, D. B. Hopkins, A. M. Sessler, and J. S. Wurtele, Phys. Rev. Lett. **57**, 2172 (1986).

[8] W. B. Colson, IEEE Jour. Quantum Electron. **QE-17**, 1417 (1981).

[9] N. M. Kroll, P. L. Morton, and M. R. Rosenbluth, IEEE J. Quantum Electron. **QE-17**, 1436 (1981).

[10]D. Prosnitz, A. Szoke, and V. K. Neil, Phys. Rev. A **24**, 1436 (1981).

[11]J. S. Wurtele, E. T. Scharlemann, and A. M. Sessler, Nucl. Instr. and Meth. **A250**, 176 (1986).

[12]J. Byers and R. Cohen, Nucl. Instr. and Meth. **A272**, 595 (1988).

[13]H. P. Freund, S. Johnston, and P. Sprangle, IEEE J. Quant. Electron. **QE-19**, 322 (1983).

[14]J. Fajans, D. Kirkpatrick, and G. Bekefi, Phys. Rev. A. **32**, 3448 (1985).

[15]J.S. Wurtele and J. Fajans, Bull. Am. Phys. Soc. **32**, 1796, 1987

[16]G. M. Branch and T. G. Mihran, IRE Trans. Elec. Dev. **ED-2**, 3 (1955).

[17]J. Fajans and J. S. Wurtele, "Profile Modification in Collective Free Electron Lasers", in press, Physics of Fluids 1989.

[18]E. Jerby and A. Gover, Nucl. Instr. and Meth. **A272**, 380 (1988).

[19]S. Y. Cai, A. Bhattacharjee, and T. C. Marshall, IEEE J. Quant. Electron. **QE-23**, 1651 (1987).

[20]R. Bonifacio, C. Pelligrini, and L. M. Narducci, Opt. Commun. **50**, 373 (1984).

[21]H. Saito and J.S. Wurtele, Phys. Fluids **30**, 2209 (1987).

[22]L. Friedland and A. Fruchtman, Phys. Rev. A **25** 2693 (1982).

[23]H. Freund and P. Sprangle, Phys. Rev. A **28**, 1835 (1983).

Figures

FIG. 1. Particle phase space (γ, ψ) (a,c,e,g) and force $(d\gamma/dz, \psi)$ (b,d,f,h) at $z = 0$ (a,b), $z = 60$cm (c,d), $z = 120$cm (e,f), and $z = 180$cm (g,h).

FIG. 2. The RF power (a) and RF phase (b) vs. interaction length z for the simulation shown in Fig. 1.

FIG. 3. Particle phase space (γ, ψ) at the end of the two meter FEL with injection at the ponderomotive velocity (zero detuning). Here $B_w = 188$G, $B_\parallel = 1510$G, $P_{in} = 4$KW, and $z = 6$m. In 3a, $I = 3.3$A. In 3b, $I = 0.01$A.

FIG. 4. Power as a function of interaction length z for three values of wiggler fields. Circles ($B_w = 243$G), crosses ($B_w = 173$G), and squares ($B_w = 115$G) are from the experiment. The lines are from simulation. Here $B_\parallel = 1450$G, $I = 3.5$A, $P_{in} = 32$KW, and $f = 9.3$GHz.

FIG. 5. Simulation of RF output power vs. interaction length z for three values of beam energy.

FIG. 6. Power vs. beam energy γ for three values of the interaction length z. The solid lines are from the experiment. The dashed lines are from simulation. Here $B_w = 187$G, $B_\parallel = 1470$G, $I = 4.5$A, $P_{in} = 32$KW and $f = 9.3$GHz.

FIG. 7. Voltage (γ) for peak gain vs. interaction length z. The dots are from the experiment and the line is from simulations. Here $B_w = 187$G, $B_\parallel = 1470$G, $I = 4.5$A, $P_{in} = 16$KW,
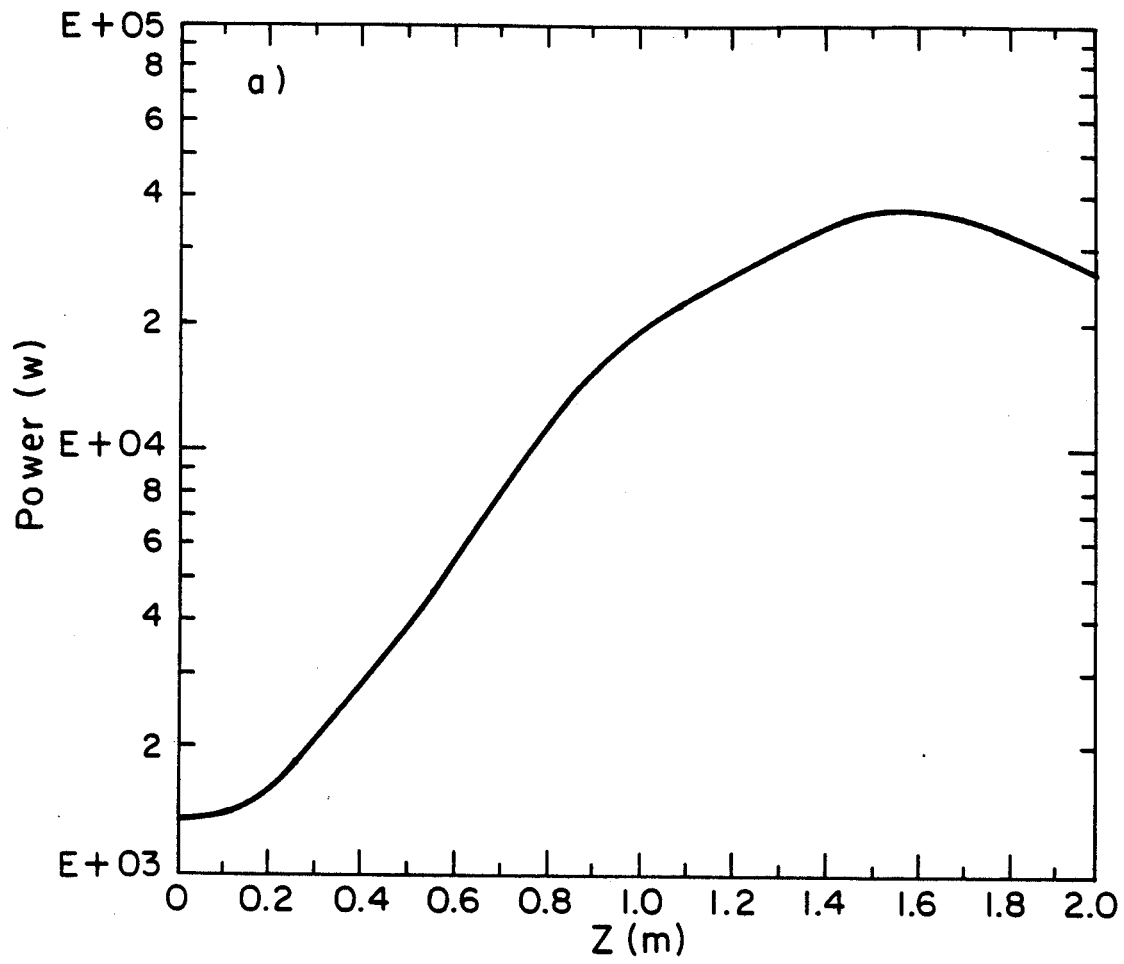
and $f = 9.3\text{GHz}$.

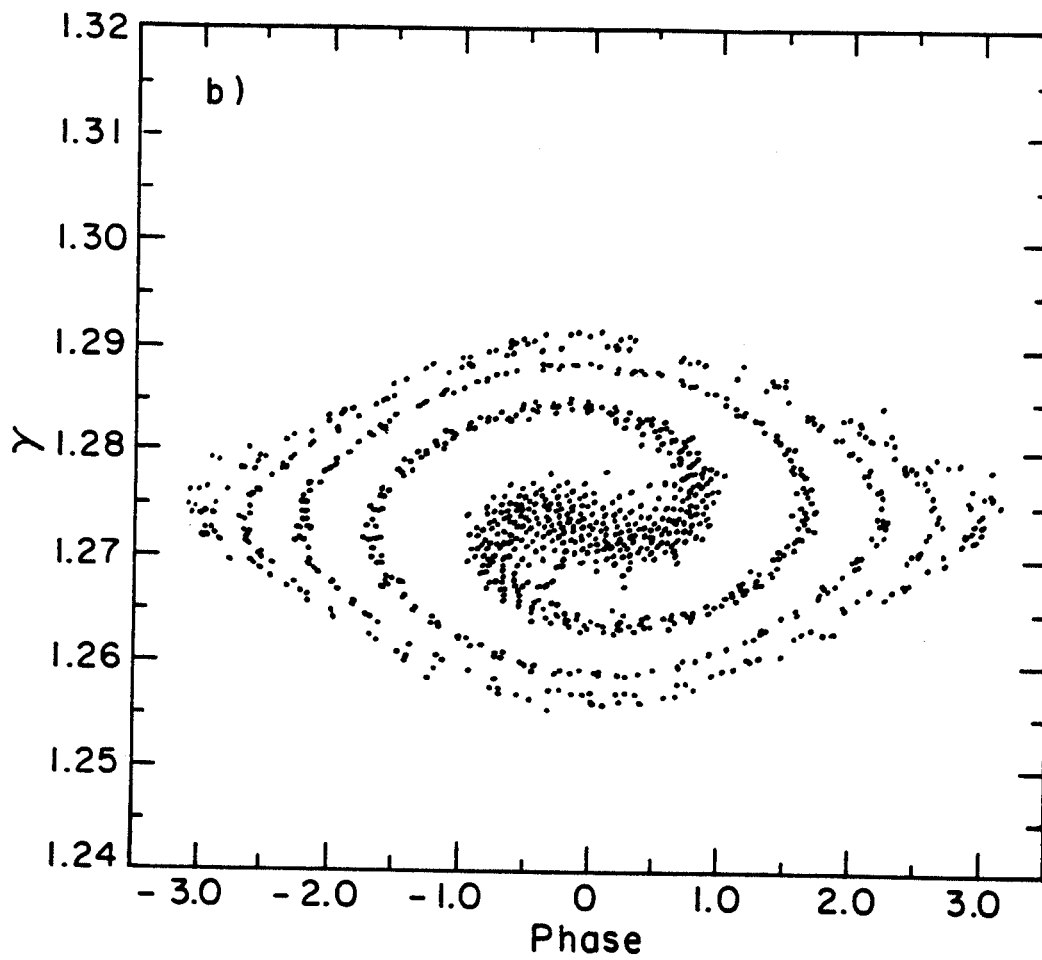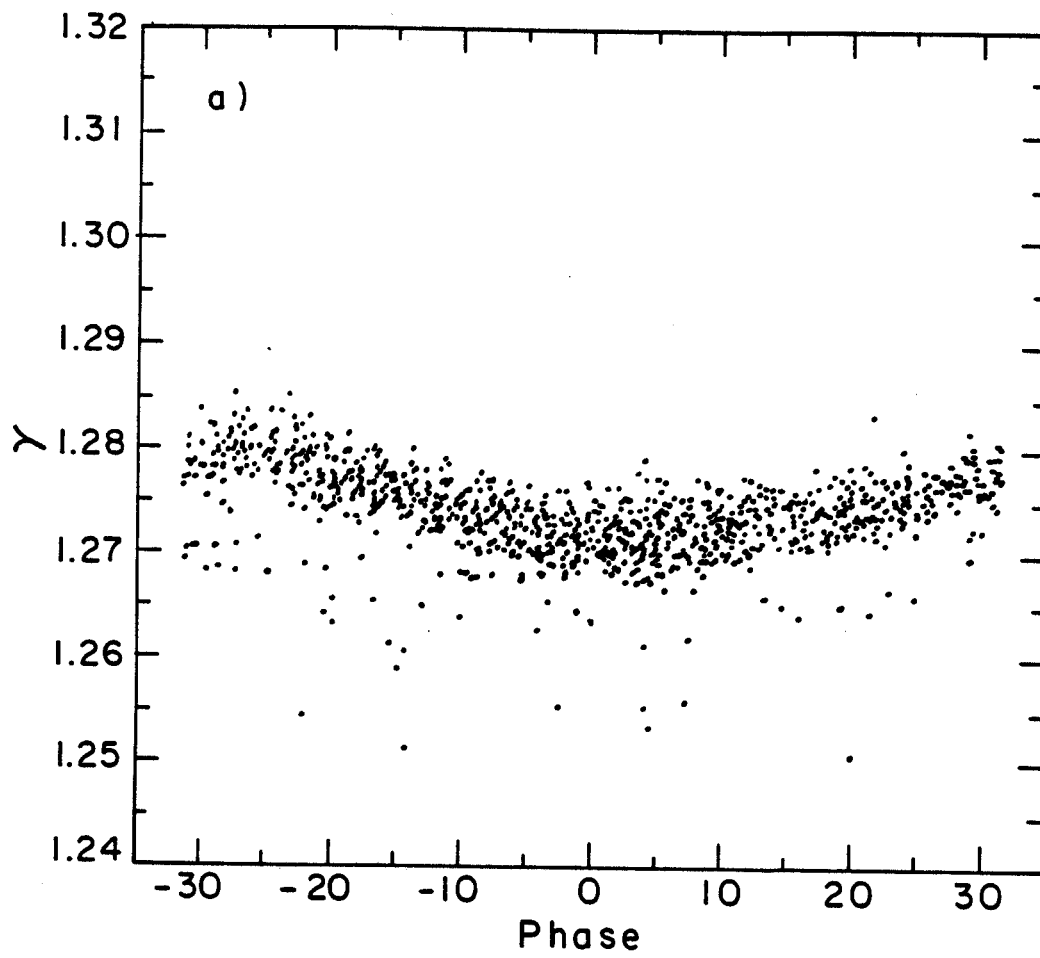FIG. 8. Schematic of the ponderomotive bucket.

FIG. 9. Normalized voltage (γ) for peak gain vs. input power P_{in}. Here $z = 115\text{cm}$, $B_w = 188\text{G}$, $B_{\parallel} = 1500\text{G}$, $I = 3.3\text{A}$, and $f = 9.3\text{GHz}$.

FIG. 10. Peak efficiency η vs. beam current I. The triangles and circles are from the simulation, and the line graphs the simplistically predicted $\eta \propto I^{1/2}$ dependence. Here $B_w = 188\text{G}$, $B_{\parallel} = 1510\text{G}$, and $f = 9.3\text{GHz}$.
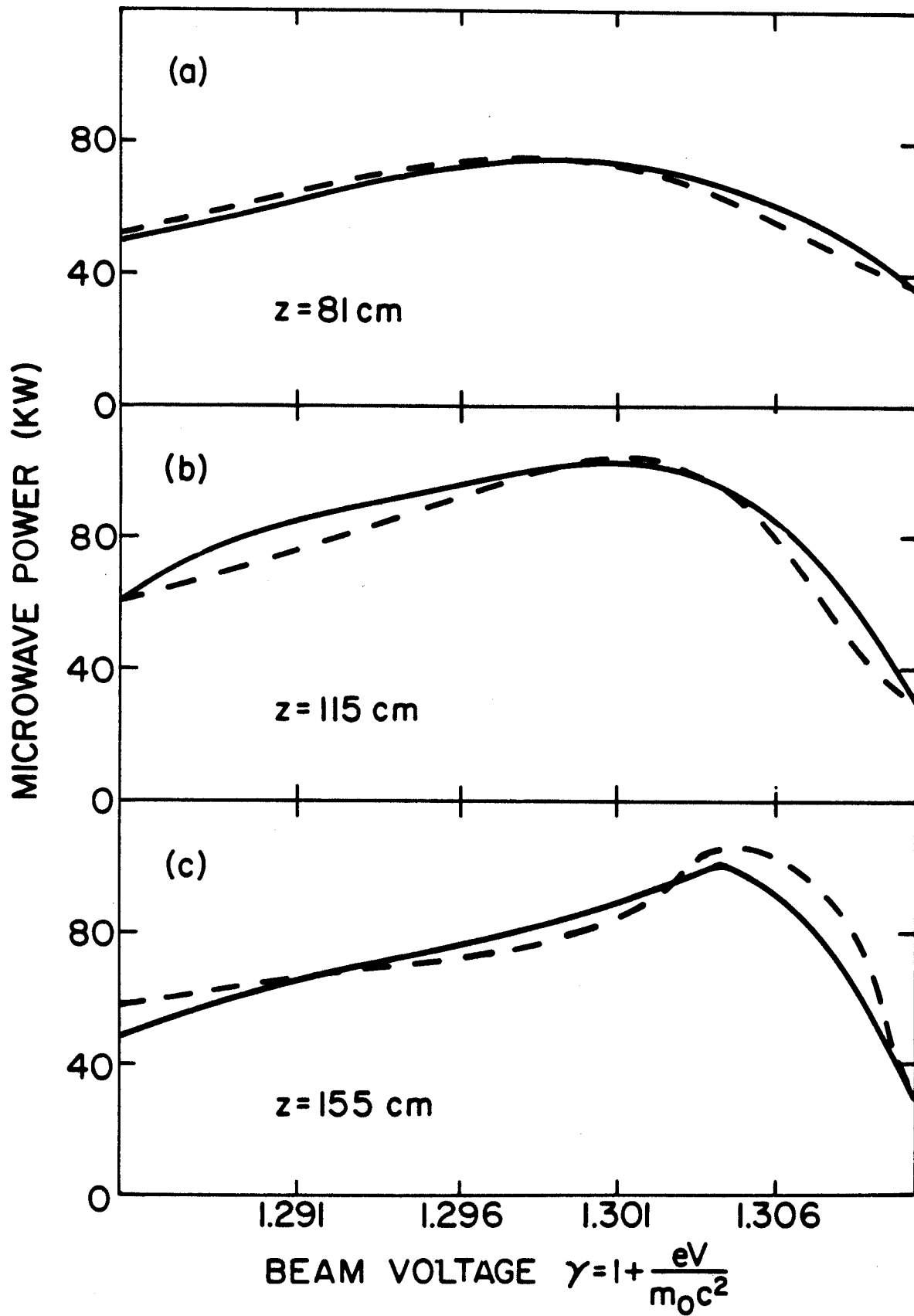
26

Fig.1 — Wurtele, Chu, Fajans

27   Fig.2 - Wurtele, Chu, Fajans

Fig.3 - Wurtele, Chu, Fajans
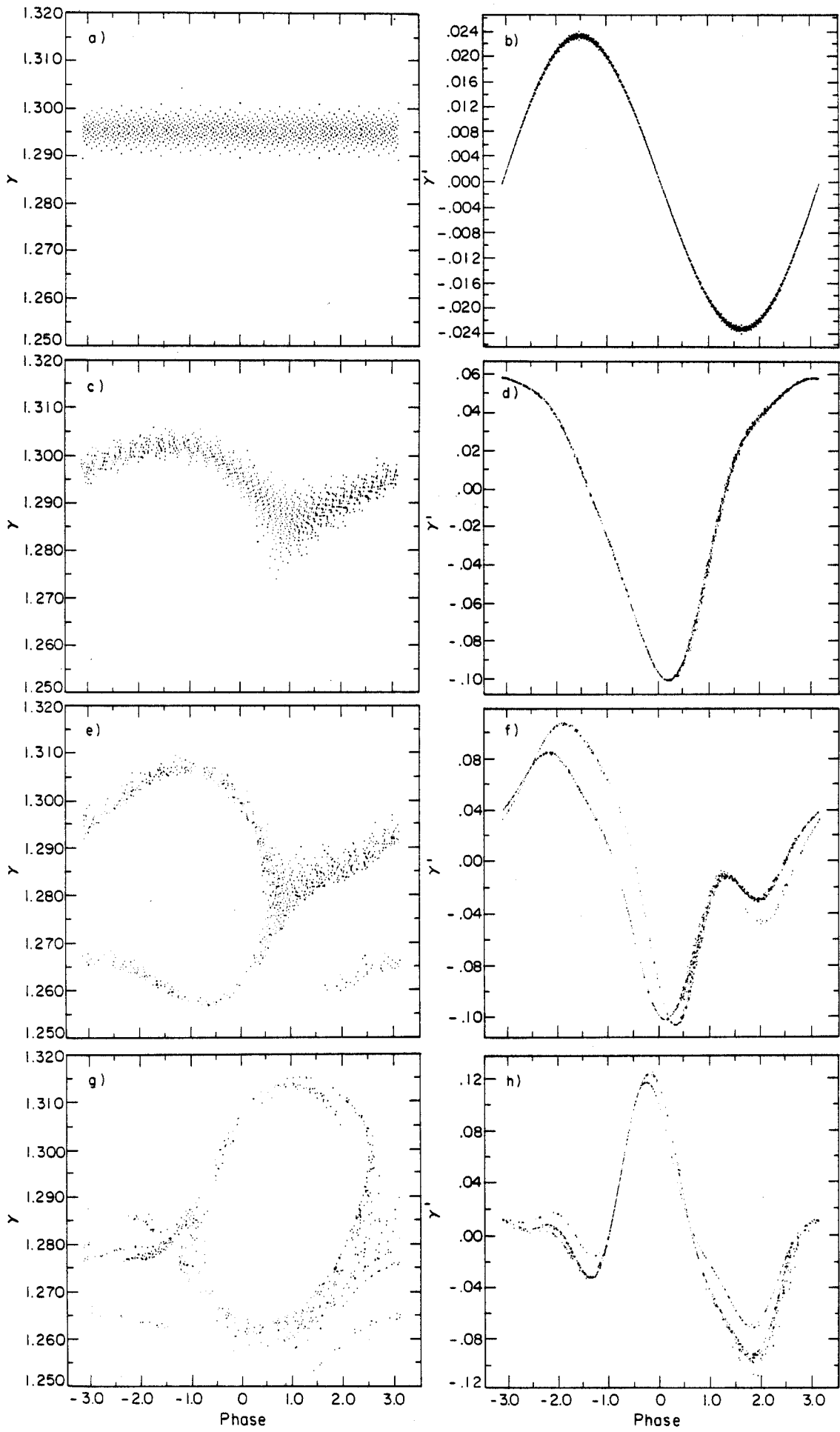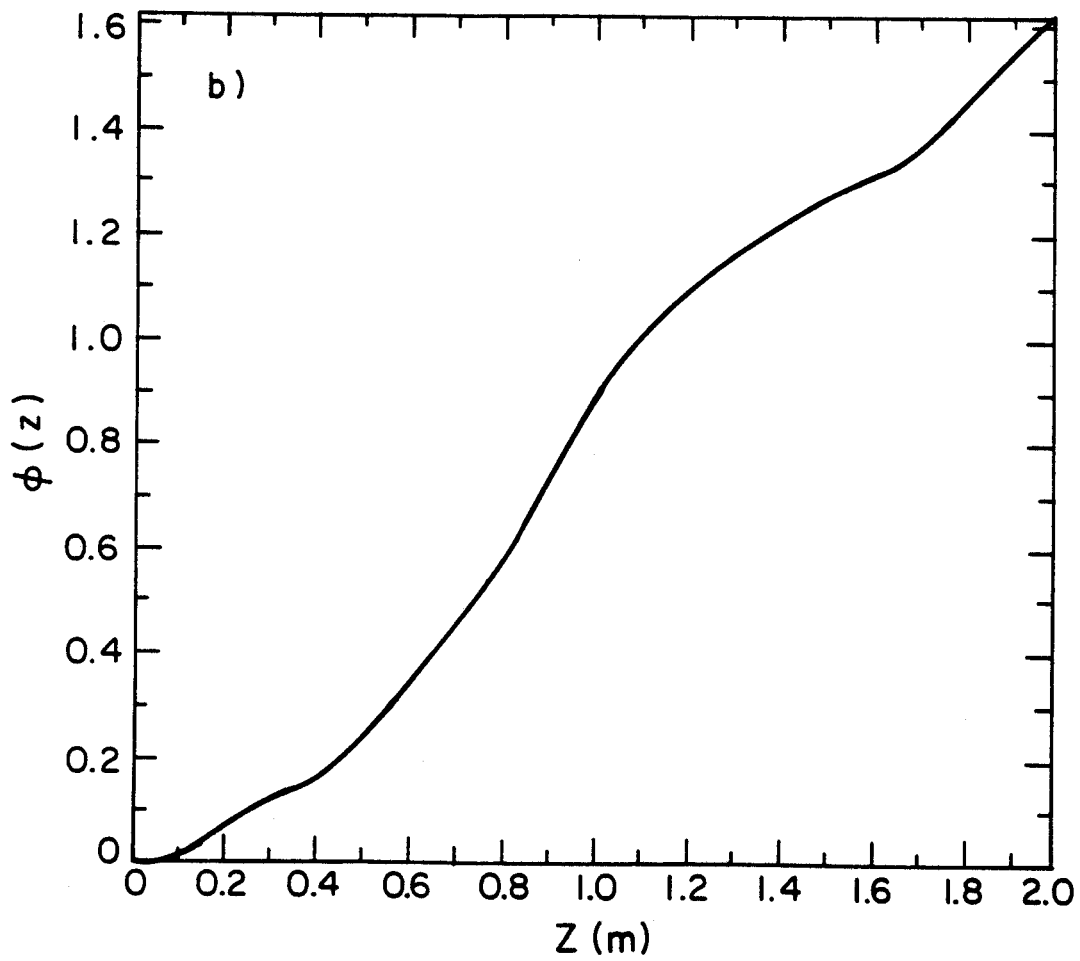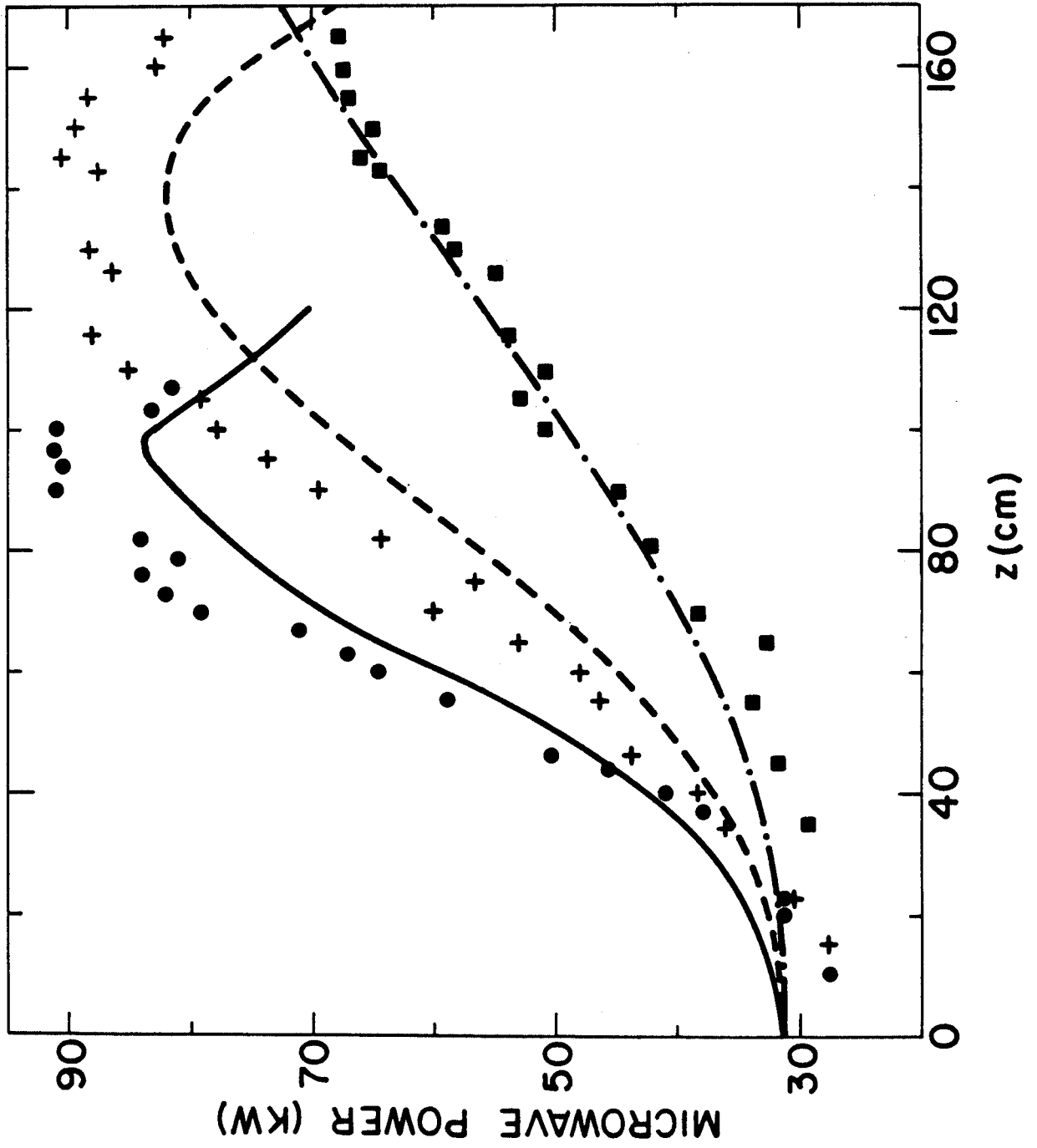
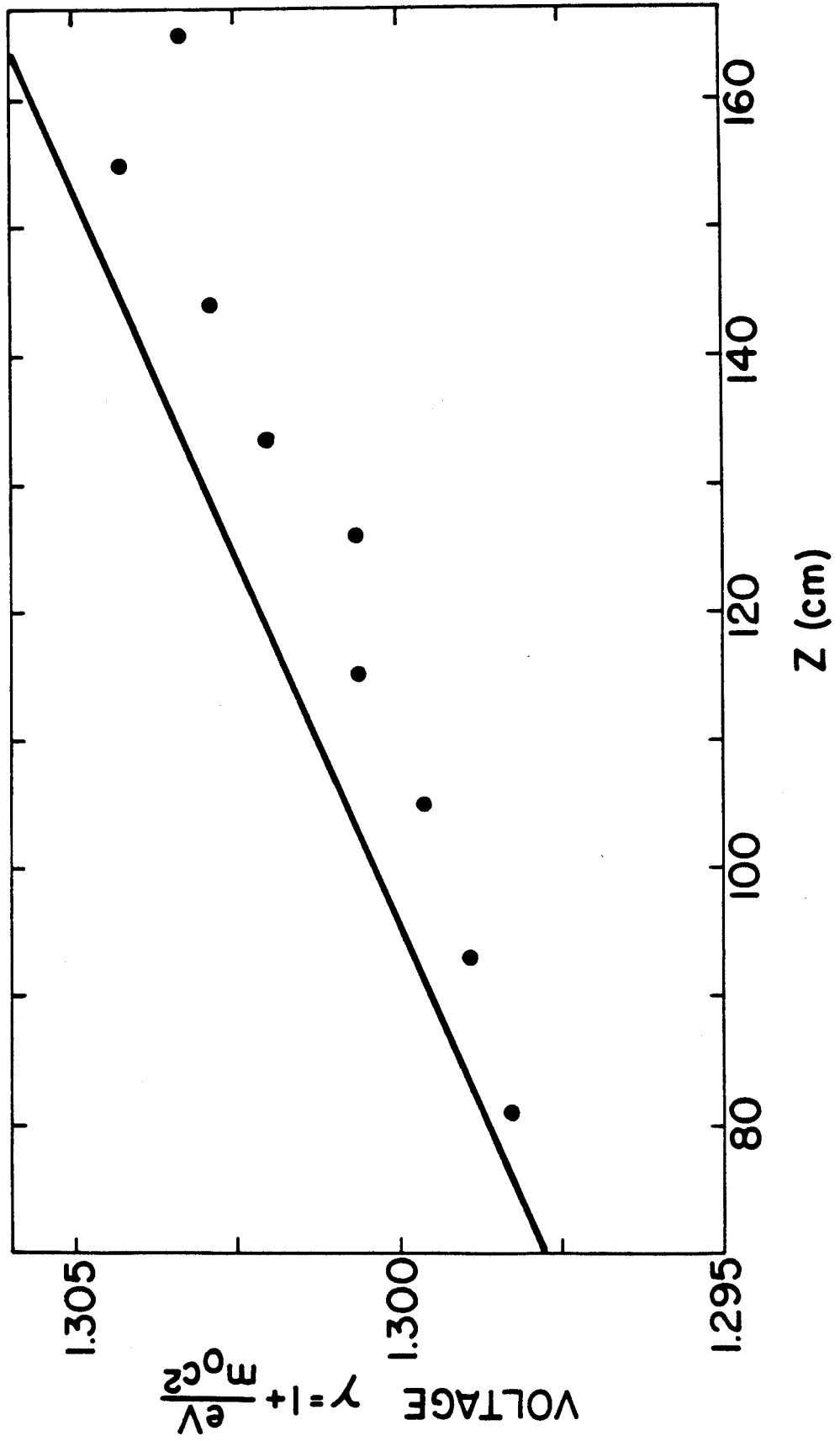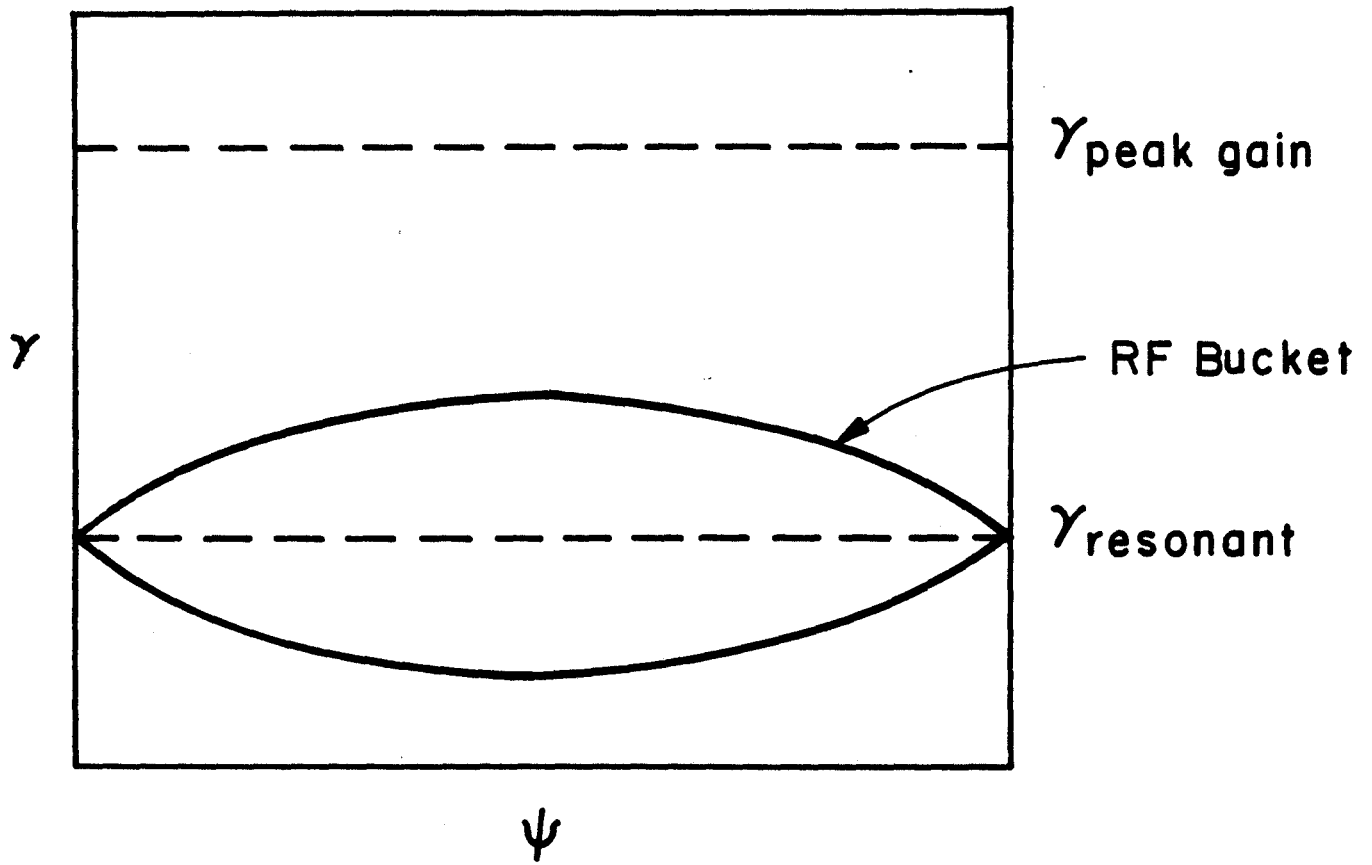Fig. 4 – Wurtele, Chu, Fajans

Fig. 5 – Wurtele, Chu, Fajans

Power (kW)

z (cm)

$\gamma = 1.306$

$\gamma = 1.308$

$\gamma = 1.300$

30

Fig.6 – Wurtele, Chu, Fajans

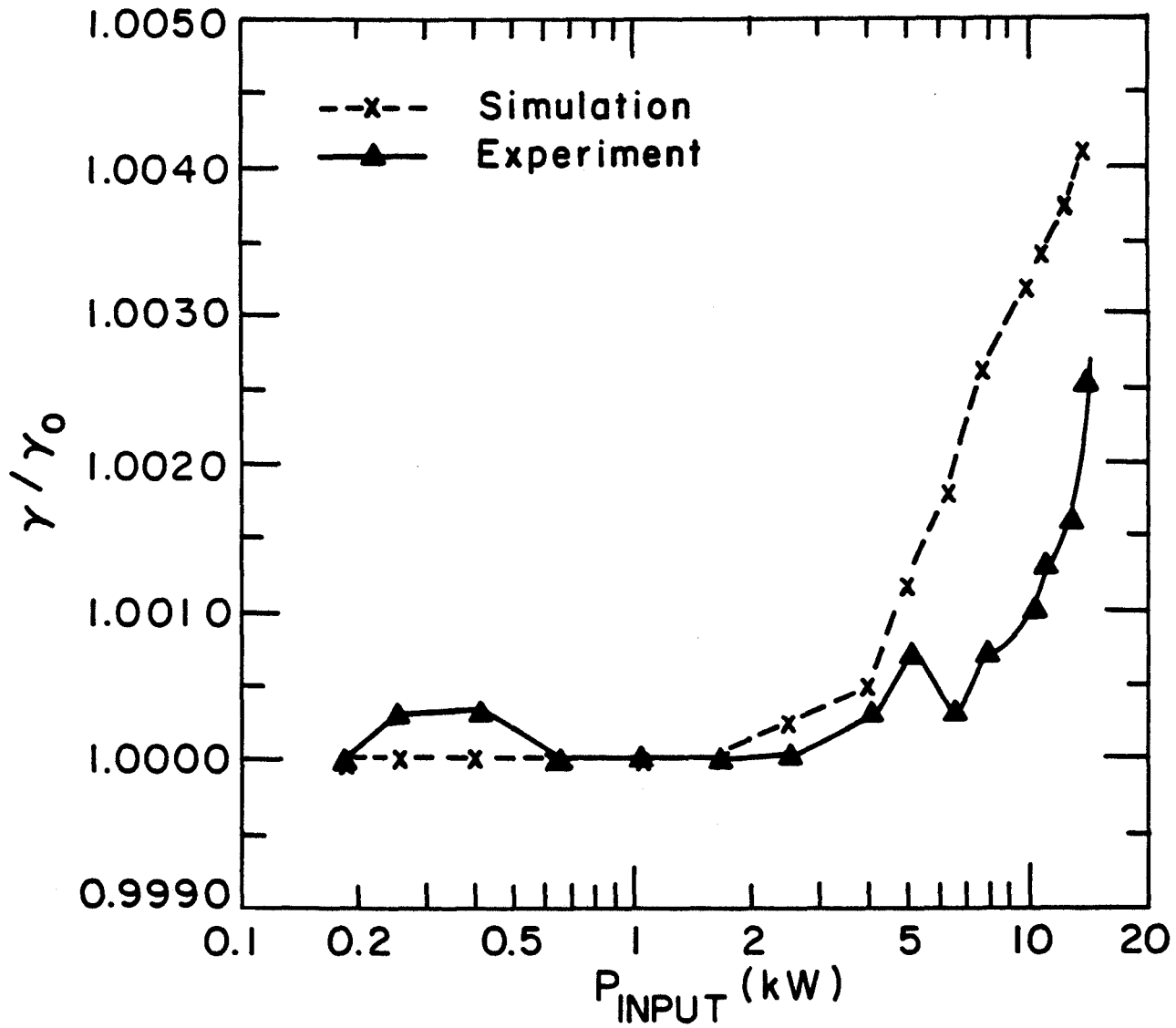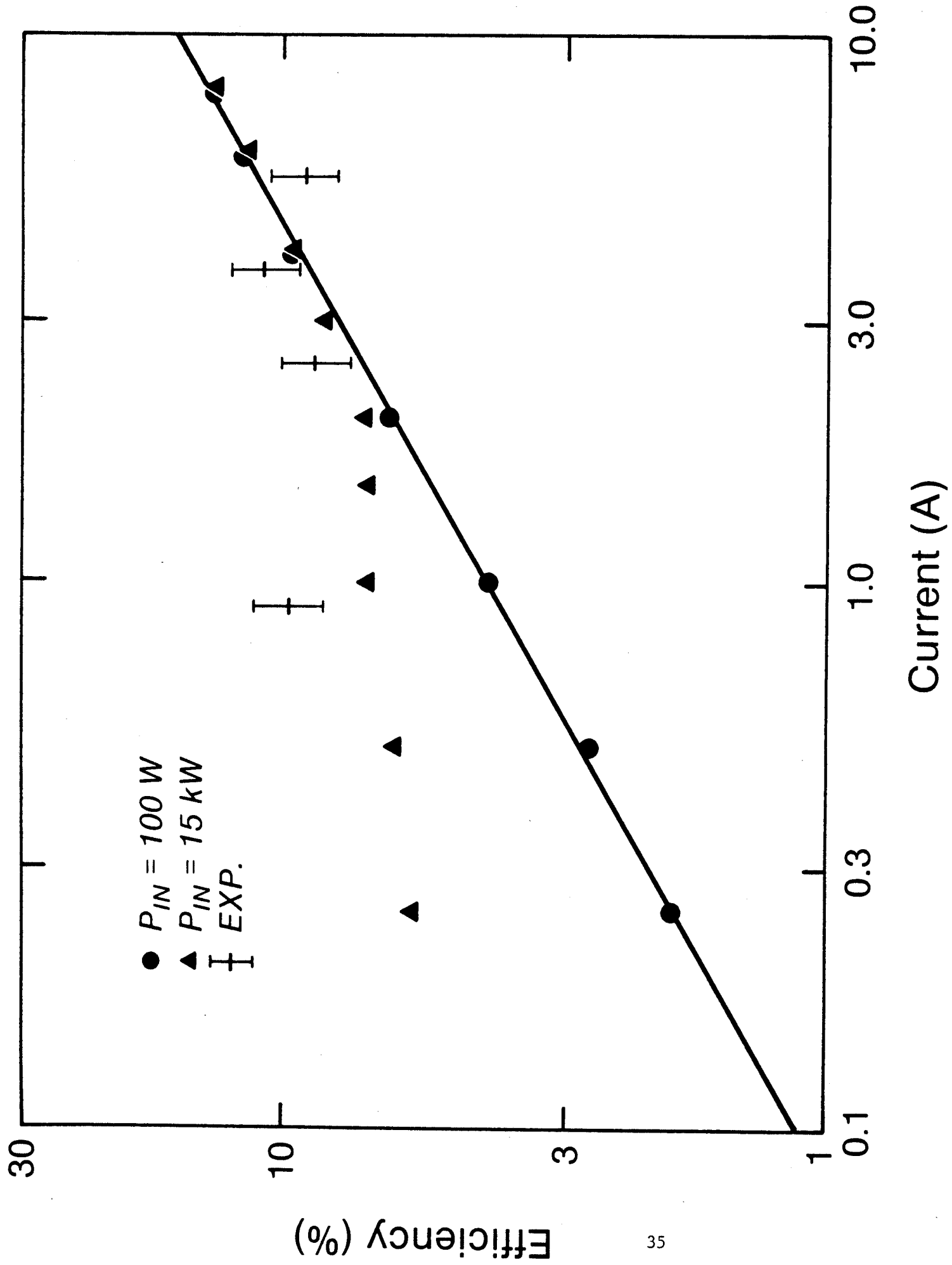Fig. 7 — Wurtele, Chu, Fajans

Fig.8 - Wurtele, Chu, Fajans

Fig.9 - Wurtele, Chu, Fajans

Fig.10 – Wurtele, Chu, Fajans